Effect of pressure on the Raman anomaly of zinc-blende CuBr and Raman spectra of high-pressure phases

F. J. Manjón, J. Serrano, I. Loa, K. Syassen,* C. T. Lin, and M. Cardona
Max-Planck-Institut für Festkörperforschung, Heisenbergstrasse 1, D-70569 Stuttgart, Germany
(Received 20 March 2001; published 11 July 2001)

Raman spectra of isotopically pure CuBr ($^{63}Cu^{81}Br$) were measured under hydrostatic pressures up to 10 GPa at 10 K. The anomalous line shape of the longitudinal-optic (LO) scattering in the zinc-blende phase (CuBr-III, 0–4 GPa), consisting of a broad structure between 155 and 177 cm^{-1}, exhibits a continuous change with pressure and develops into a narrow LO phonon peak near 4 GPa. The disappearance of the LO Raman anomaly as well as the pronounced broadening of the TO mode with pressure are explained in terms of pressure-dependent third-order anharmonic interactions with two-phonon states. A Fermi resonance model, which is based on a shell model fit of available phonon dispersion data, fully accounts for the changes in Raman line shapes under pressure. Low-temperature Raman spectra of the tetragonal CuBr-IV and cubic CuBr-V high-pressure phases are also reported. An assignment of the observed Raman modes of these phases is proposed.

DOI: 10.1103/PhysRevB.64.064301 PACS number(s): 63.20.Kr, 62.50.+p, 78.30.−j

I. INTRODUCTION

Anomalous features in the first-order Raman spectra of several zinc-blende (ZB) semiconductors have recently attracted attention and were studied experimentally[1–6] and in theoretical work.[7–10] Usually, Raman spectra of undoped zinc-blende compounds measured under nonresonant conditions show two narrow spectral features corresponding to scattering by zone-center ($\mathbf{q}=0$) transverse-optical (TO) and longitudinal-optical (LO) phonons. In the case of GaP the TO Raman line is asymmetric and significantly broader than the LO peak.[4,5,11] A more pronounced anomaly is seen in CuCl where the Raman scattering with transverse-optic (TO) polarization characteristics at frequencies below the LO line shows a broad multipeak feature. While the anomalous TO scattering of CuCl was early noted[12,13] and studied extensively,[1–3,14–19] no indication was originally reported for anomalies in the first-order Raman spectra of CuBr measured at 4 K.[20–22] However, detailed Raman studies of CuBr as a function of isotopic composition[6] have revealed that the LO scattering consists of a band with several spectral features, showing a pronounced dependence on isotopic composition.

Two explanations for Raman anomalies in copper halides have been discussed, in particular for the TO feature in CuCl. They are based on the off-center model[7–9,17–19] and the Fermi resonance model (FRM).[14–16,23] In the off-center model one considers a disordered Cu^+ sublattice with a fraction of the Cu^+ ions located in off-center minima of the lattice potential. This may lead to local modes associated with different positions for the Cu^+ ions. Recent *ab initio* total-energy calculations[7,8] and molecular-dynamics simulations[9] for CuCl indicate the possibility of stable or metastable static off-center displacements or dynamical disorder of Cu ions at low temperatures. In the FRM, one considers a renormalization of the TO(Γ) phonon due to anharmonic interactions with a two-phonon continuum. Low-temperature Raman measurements on CuCl as a function of isotopic composition[1,2] and hydrostatic pressure[3,24] have proven to be an effective means to experimentally discriminate between the two different explanations for the Raman anomaly and provide strong support for the FRM. Similarly, all experimental results concerning the Raman anomalies of GaP[1,2,5,11] and CuBr[6] are consistent with the Fermi resonance picture. The pressure-induced narrowing of the TO peak in GaP is also very well reproduced by first-principles calculations of the anharmonic decay of the $\mathbf{q}=0$ TO phonon.[10]

In this work we are mainly interested in the anomalous LO Raman feature in CuBr. We report Raman spectra of CuBr single crystals measured at $T=10$ K under hydrostatic pressures up to 4 GPa. This pressure value marks the stability limit for the ZB phase (CuBr-III) at low temperatures. Despite this narrow stability range, the application of pressure allows one to tune phonon frequencies of ZB CuBr over a much wider range as compared to isotope substitution. The LO scattering of CuBr is found to be strongly pressure dependent. With increasing pressure it develops into a narrow spectral feature. On the other hand, the TO mode is found to broaden significantly with increasing pressure. We show that the high-pressure behavior of the TO and LO Raman features in CuBr are fully reproduced by a FRM. Our FRM simulation of pressure-dependent Raman spectra of CuBr involves a realistic shell model for the phonon dispersions and phonon density of states. The present results for ZB CuBr represent an important example of pronounced anharmonic effects in the Raman spectra of copper halides.

Besides the ZB phase of CuBr we have also studied two high-pressure modifications. On the Phillips scale,[25] the copper halides have ionicity values which are near the stability limit separating four- and six-coordinated structures. These compounds, however, do not directly transform to six coordination under pressure. Instead, optical and structural studies have revealed a more complex phase transition behavior, involving intermediate four-coordinated structures preceding the transition to a rocksalt phase.[26–34] Here, we report low-temperature Raman spectra of the tetragonal antilitharge (litharge is PbO) phase CuBr-IV (4.0–7.2 GPa) and the cubic (SC16-type) phase CuBr-V (6.3–8.8 GPa). Based on measured mode frequencies, their mode Grüneisen parameters,

and a comparison with Raman spectra of structurally related copper halide phases,[27,29,34] we propose an assignment of the Raman-active modes observed for the high-pressure phases of CuBr.

II. EXPERIMENT

Crystals of $^{63}Cu^{81}Br$ were grown by vapor transport from isotopically pure (99%) ^{63}Cu and ^{81}Br as described in Ref. 35. The samples were platelets having [111] orientation and a thickness of less than 30 μm. They were cut into pieces of about 100×100 μm in size and fitted into the hole of the gasket of a diamond anvil cell (DAC). Helium was used as a pressure transmitting medium in order to ensure fully hydrostatic conditions at low temperatures (10 K) and to avoid chemical reactions. Before changing pressure, the cell was always heated to a temperature above the melting point of helium in order to keep stresses as low as possible. The pressure was measured by the ruby luminescence method[36,37] using a temperature correction according to Ref. 38. Raman experiments were performed in backscattering geometry with the 647.1-nm line of a Kr^+-ion laser. In order to avoid sample heating, the incident light intensity was kept below 200 W/cm^2. The scattered light was analyzed by a Jobin-Yvon T64000 spectrometer in combination with a multichannel charge-coupled device (CCD) detector. The spectral resolution determined from the full width at half maximum (FWHM) of Ne calibration lines was 1.4 cm^{-1}.

III. ZINC-BLENDE PHASE

Figure 1 shows Raman spectra of ZB-CuBr (CuBr-III) at different pressures at $T=10$ K. The line width of the TO structure, located at 136.3(2) cm^{-1} at zero pressure, increases considerably with pressure. At the highest pressure a shoulder develops on its high-frequency side. The LO structure extends from about 155 to 177 cm^{-1} and shows three components, labeled as γ, β, and η in Fig. 1. The LO band exhibits pronounced changes under pressure. The intensity of the broad peak β, centered at 167.9 cm^{-1} at $P=0$, decreases whereas that of the high-energy feature γ, located at 173.5 cm^{-1} at $P=0$, increases and develops into a rather narrow peak.

For a quantitative characterization of the pressure-induced spectral changes we have fitted Voigt profiles to the experimental spectra. These are Lorentzians convoluted with a Gaussian with a FWHM corresponding to the spectrometer resolution. The LO signal has been modeled by a superposition of three Voigt components (γ, β, η). Figure 2 shows the obtained peak frequencies as a function of pressure. The corresponding pressure coefficients are listed in Table I. The mode Grüneisen parameters of the TO and LO-(γ) features (see Table I) are similar to those of the TO and LO modes in the ZB phases CuCl-II (1.9 and 1.5 at 5 K, Ref. 3) and CuI-III (2.08 and 1.44 at 100 K, Ref. 29). The LO(γ)-TO splitting as a function of pressure is shown in Fig. 3, together with the difference in the corresponding TO and LO bare (harmonic) frequencies discussed below. The decrease of the splitting with pressure is typical for most polar tetrahedral

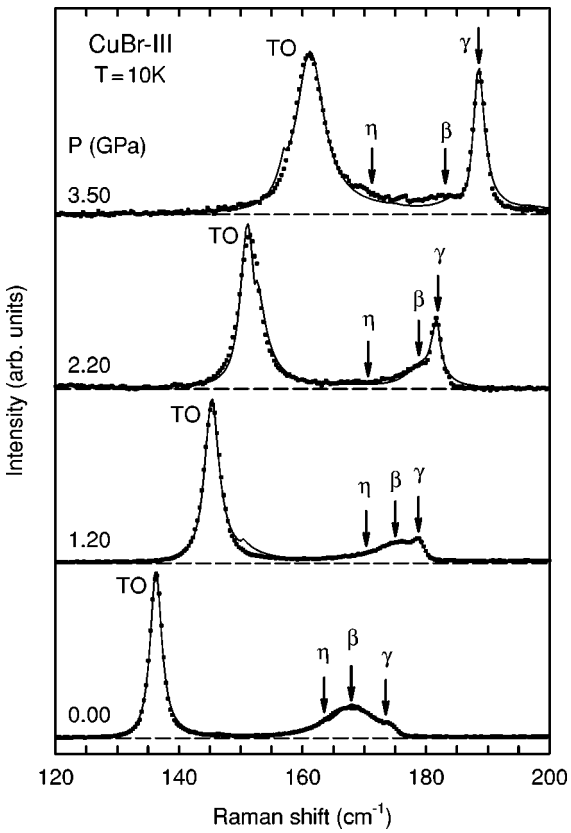

FIG. 1. Low-temperature Raman spectra of zinc-blende $^{63}Cu^{81}Br$ measured at different pressures up to 4 GPa (solid symbols). The spectra are normalized with respect to the height of the TO peak. Solid lines correspond to fits of a Fermi resonance model (see text).

semiconductors and mainly reflects a decrease of the Born transverse dynamic effective charge.[39,40] The width of the TO band of CuBr (Fig. 4) increases by a factor of 4 in the 0–4-GPa range, whereas that of the LO(γ) feature shows a weak increase, but only at pressures above ~2 GPa.

All frequency shifts and changes in linewidths observed under pressure were fully reversible. This also applies to an experimental run extending into the four-coordinated phases CuBr-IV and CuBr-V. Only after a transition into the rocksalt phase the widths of the spectral features of the ZB phase were substantially modified upon releasing pressure, possibly due to irreversible generation of defects. In all spectra taken for samples inside the DAC (with helium medium) the ratio between the integrated intensities of the LO and TO features remained constant (0.35 ± 0.05), independent of pressure. A different ratio (0.65) has been obtained at $P=0$ for a free-standing sample. This is probably the result of differences in the scattering geometries for all collected scattered rays.

Raman line shapes similar to those observed for CuBr were obtained in early calculations of anharmonic interactions of $\mathbf{q}=0$ optical phonons with acoustic $\mathbf{q}=0$ two-phonon states.[41] Furthermore, pressure-dependent spectral changes qualitatively similar to those of the LO feature in CuBr have been observed for the TO-like structure of CuCl.[3,24,42] In this case, the pressure-induced major changes of the TO Raman feature are well accounted for by a FRM.[3]

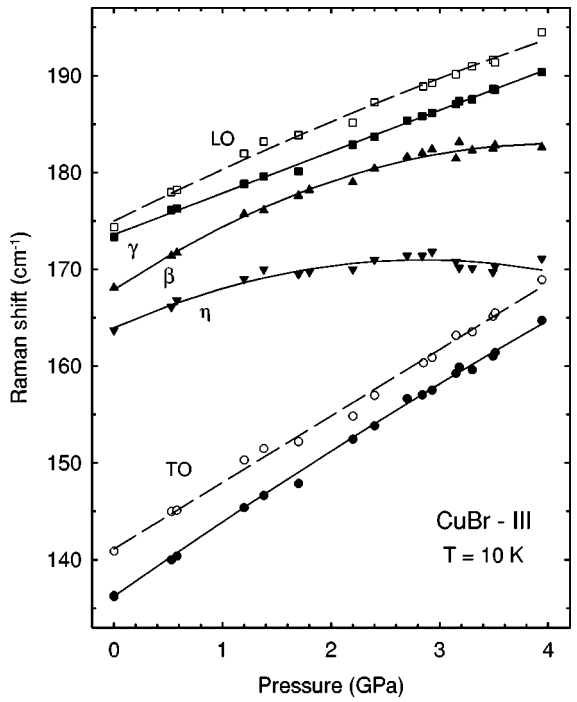

FIG. 2. Frequencies of the Raman peaks of zinc-blende $^{63}Cu^{81}Br$ as a function of pressure (solid symbols). The bare (harmonic) TO and LO frequencies obtained by fitting a Fermi resonance model (see text) are shown by open symbols.

The large broadening of the TO feature of CuBr under pressure indicates that the TO-like scattering may also be strongly affected by pressure-dependent anharmonic effects. We show here that a FRM, based on a realistic two-phonon density of states for $\mathbf{q}=0$, accounts well for the evolution of both the TO *and* LO Raman features of CuBr as a function of pressure.

The Raman spectrum $I(\omega)$ as a function of frequency ω can be expressed as[43,44]

$$I(\omega)\propto\frac{\Gamma(\omega)}{[\omega-\omega_b-\Delta(\omega)]^2+\Gamma^2(\omega)}. \tag{1}$$

TABLE I. Pressure shifts of the Raman peak frequencies of CuBr-III at 10 K. Coefficients were obtained by fitting quadratic relations to the data. The frequencies ω_0 of the Raman peaks are given at 1 atm and the mode Grüneisen parameters were derived using a bulk modulus value of $B_0=36.6(8)$ GPa (Ref. 32).

Peak	ω_0 (cm^{-1})	$d\omega/dP$ (cm^1/GPa)	$\frac{1}{2}d^2\omega/dP^2$ (cm^{-1}/GPa^2)	γ_G
TO	136.3(5)	7.7(3)	−0.13(5)	2.05(6)
η	163.9(6)	4.9(4)	−0.87(4)	
β	167.9(8)	7.4(3)	−0.91(3)	
γ	173.5(5)	4.3(2)	−0.02(1)	0.91(6)
TO (bare)	141.5(5)	7.0(4)	0 (fixed)	1.83(9)
LO (bare)	175.0(5)	5.8(2)	0 (fixed)	1.21(8)

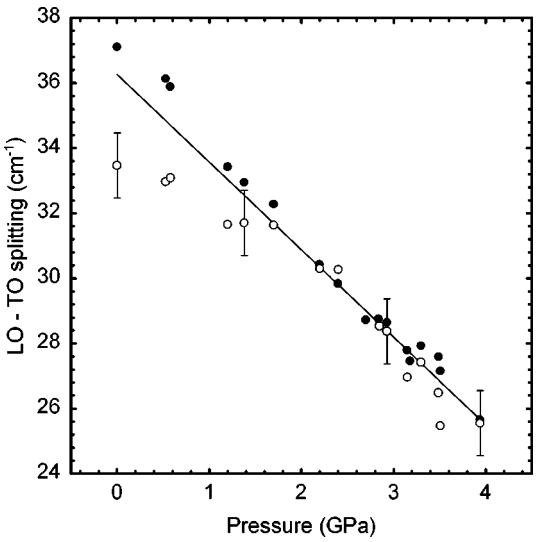

FIG. 3. Observed splitting between the LO(γ) and TO peaks (closed dots) of CuBr as a function of pressure. The solid line represents a linear regression of the data above 2 GPa. Differences between the bare (harmonic) LO and TO frequencies are represented by open symbols.

Here ω_b is the bare (harmonic or unrenormalized) phonon frequency and $\Gamma(\omega)$ and $\Delta(\omega)$ are the frequency-dependent imaginary and real parts, respectively, of the low-temperature phonon self-energy. Real and imaginary parts are related through a Hilbert transformation (except for a difference in sign this corresponds to a Kramers-Kronig transformation). In this work, we consider a third-order perturbation approach (coupling of an optical phonon to two phonons of lower energy) to account for the anharmonic contribution to phonon linewidths and frequencies. The anharmonic broadening $\Gamma(\omega)$ is proportional to the $\mathbf{q}=0$ two-phonon density of states $\rho(\omega)$,

$$\Gamma(\omega)=\frac{18\pi}{\hbar^2}|V_3|^2\rho(\omega)\equiv A\rho(\omega). \tag{2}$$

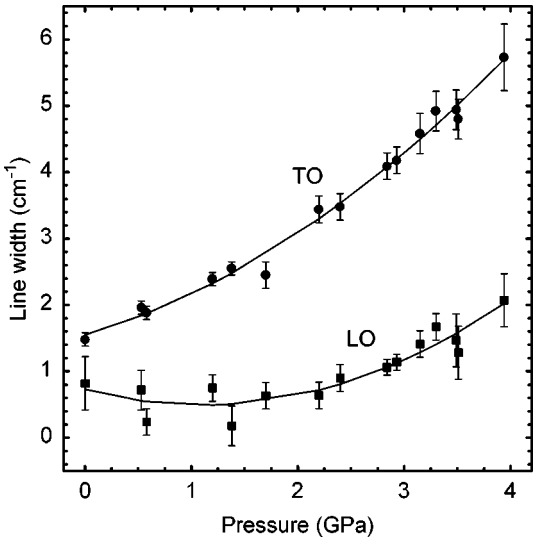

FIG. 4. Full widths at half maximum of the LO(γ) and TO peaks as a function of pressure. Lines represent guides to the eye.

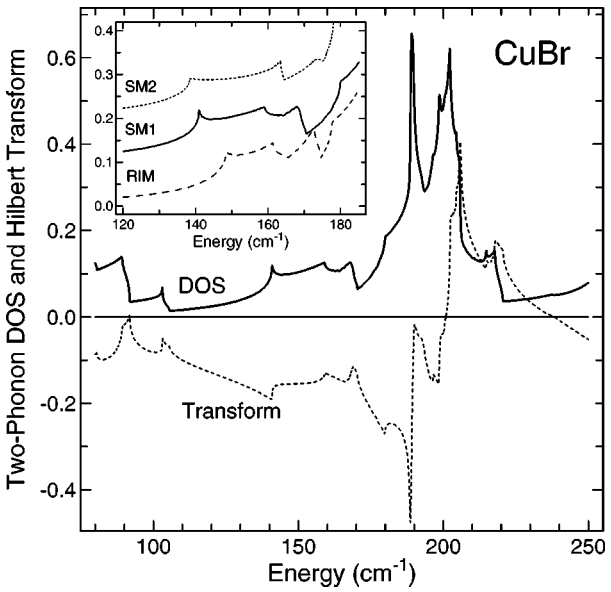

FIG. 5. Zero wave vector two-phonon density of states and its Hilbert transform at ambient pressure as calculated with the shell model (SM1) of Ref. 45. The inset shows a selected range of the two-phonon DOS calculated with the rigid ion model (RIM) after Ref. 46 and the shell models SM1 and SM2 after Ref. 45. For clarity, a vertical offset is used in the inset. The sharp structures located near 141, 159, 168, and 180 cm^{-1} in the shell model SM1 correspond to TA+LA combinations at the L, W, and K points of the Brillouin zone and to the TA+TO combination at the K point, respectively.

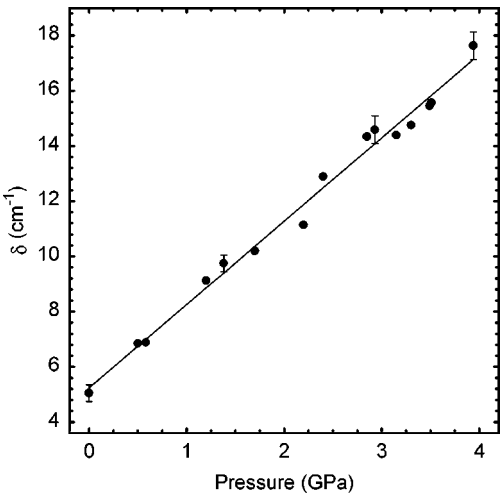

FIG. 6. The rigid shift δ applied to the two-phonon DOS of the shell model SM1 as a function of pressure. The slope approximately represents the pressure shift of TA(K)+LA(K) combinations of CuBr.

The squared third-order matrix element $|V_3|^2$ is a measure of the coupling strength between a $\mathbf{q}=0$ optical phonon and $\mathbf{q}=0$ two-phonon combinations. We assume, as is often done, that $A=(18\pi/\hbar^2)|V_3|^2$ is independent of frequency. Thus, for a given two-phonon density of states and coupling strength, the Raman spectrum can be readily calculated.

We have modeled the two-phonon density of states (DOS) using parameter sets for a shell model (SM1 and SM2) and a rigid-ion model (RIM). These models were used to fit the phonon dispersion curves obtained from inelastic neutron-scattering measurements.[45,46] Figure 5 shows the two-phonon DOS of CuBr at $P=0$ and its Hilbert transform, as calculated with the shell model SM1.[45] The inset of Fig. 5 shows the two-phonon DOS for the SM1 and SM2,[45] and for the RIM,[46] limited to the frequency range of interest here. While all three models exhibit similar overall features, there are differences of a few wave numbers in the frequencies of two-phonon DOS maxima and edges.

We have tested all three models in the simulation of the ambient pressure Raman spectrum. In these simulations we have allowed for a small rigid frequency shift δ of the calculated two-phonon DOS, i.e., $\rho(\omega)$ in Eq. (2) is replaced by $\rho(\omega-\delta)$. The best overall agreement with the $P=0$ experimental Raman spectrum is obtained for the SM1 with $\delta=5$ cm^{-1}. This is not surprising because the SM1 gives the best description of the acoustic phonon dispersion curves at the W and K points of the Brillouin zone (BZ).[45] Therefore the SM1 description was used for the simulation of the high-pressure Raman spectra. We have assumed that, to a first approximation, we can account for the effect of pressure on the two-phonon DOS in the relevant frequency region by allowing for a pressure-dependent rigid shift δ.

For fitting the LO-like broad band shown in the experimental spectra, we have used Eqs. (1) and (2) with four free parameters: the bare LO phonon frequency ω_b, the rigid shift δ of the two-phonon DOS and its Hilbert transform, the coefficient A, and an intensity scaling factor. The TO feature was fitted in a similar way. Due to the lack of asymmetry or additional structure near the TO Raman feature, the value of the δ parameter is less well constrained in this case. Therefore for the TO feature we have used only three free parameters, fixing the two-phonon DOS shift δ to that obtained for the LO mode at the same pressure value. The solid lines in Fig. 1 represent fitted spectra. A very good agreement is found at lower pressures. Towards higher pressures, the agreement is less perfect. This, however, is not surprising in view of our simple approximation according to which the frequencies of all relevant acoustic phonon combinations shift at the same rate $d\delta/dP$.

The dependence on pressure of the rigid shift δ of the two-phonon DOS is shown in Fig. 6. The average linear shift amounts to 3.25 cm^{-1}/GPa. This value is smaller than the pressure coefficients of the TO and LO frequencies. It implies that the relevant combinations of $\mathbf{q}=0$ two-phonon states shift at a smaller rate compared to optical phonons. It involves one TA phonon which has a negative frequency shift with increasing pressure. Figure 7 shows the coupling coefficient A for the TO and LO modes as a function of pressure. The fits of the TO structure yield only a small variation of A(TO) with an average value of 25 ± 5 cm^{-2}. For the LO peak, however, a decrease of A with increasing pressure is inferred from our fits of the experimental spectra.

The bare TO and LO phonon frequencies, and their splitting as obtained from the fits, are indicated by open symbols in Figs. 2 and 3. The corresponding pressure coefficients and mode Grüneisen parameters are given in Table I. The LO-TO

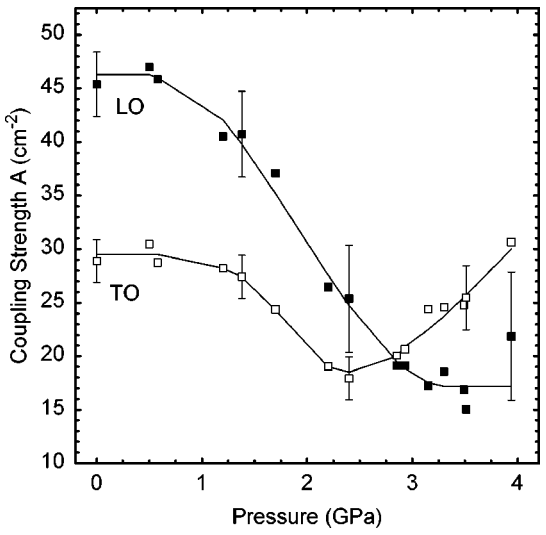

FIG. 7. Coupling strength $A=(18\pi/\hbar^2)|V_3|^2$ for the anharmonic third-order interaction of TO and LO modes as a function of pressure. Solid lines are guides to the eye.

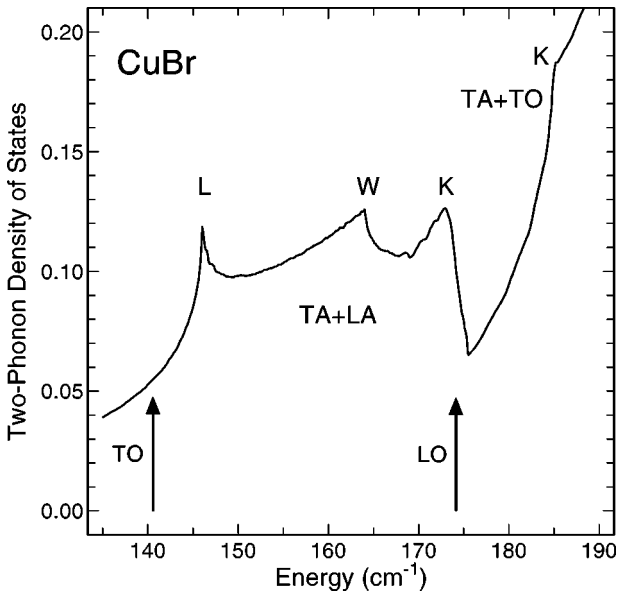

FIG. 8. Two-phonon density of states at zero pressure as calculated with the parameters of the shell model SM1 (Ref. 45), but rigidly shifted by $\delta=5$ cm^{-1}. The assignment of the DOS singularities to the two-phonon combinations at high-symmetry points of the Brillouin zone is indicated. Arrows mark the harmonic frequencies of the TO and LO phonons at zero pressure.

splitting of the bare phonon frequencies decreases at a rate which is somewhat smaller than that for the measured LO(γ) and TO features. Using the values of the Grüneisen parameters of the harmonic (unrenormalized) frequencies it is possible to obtain the Grüneisen parameter of the transverse dynamic effective charge

$$e^*=\left[\frac{\epsilon_\infty \mu V_m}{4\pi}(\omega_{LO}^2-\omega_{TO}^2)\right]^{1/2}. \tag{3}$$

The quantities μ and V_m are the reduced effective mass and volume per formula unit, respectively, and ϵ_∞ (ϵ_0) is the high-frequency (static) infrared dielectric constant. From the harmonic TO and LO frequencies we obtain $e^*=1.23$, using $\epsilon_\infty=4.37$, from Ref. 47. The negative logarithmic derivative of e^* with respect to the volume is

$$\gamma^*=-\frac{d\ln e^*}{d\ln V}=\gamma_{LO}+\frac{(\gamma_{LO}-\gamma_{TO})\omega_{TO}^2}{\omega_{LO}^2-\omega_{TO}^2}+\frac{1}{2}\gamma_\infty-\frac{1}{2}. \tag{4}$$

The value of $\gamma_\infty=-d\ln\epsilon_\infty/d\ln V$ is -0.2 according to Ref. 39. From Eq. (4) and the harmonic Grüneisen parameters of Table I we then obtain $\gamma^*\simeq-0.6$, which is similar to typical values found for the III-V compounds ($\gamma^*\simeq-0.6$ for InP, see Ref. 40). The negative sign, which corresponds to a decrease in the transverse dynamic effective charge with decreasing volume, is found for most III-V and II-VI compounds, the only exception being SiC.[48] The harmonic frequencies are the correct ones to be used in the determination of e^* and γ^*. Our value of γ^* differs significantly from that obtained with the renormalized TO and LO(γ) frequencies ($\gamma^*=-1.6$).

The pressure dependence of the linewidths (Fig. 4) and the coupling strengths (Fig. 7) can be understood if we trace in more detail the position of the bare phonon frequencies relative to the two-phonon DOS (see Fig. 8). The marked structures located at about 146, 164, 173, and 185 cm^{-1} in the shifted SM1 DOS correspond to TA+LA combinations at the L, W, and K points of the Brillouin zone (BZ) and to TA+TO at the K point, respectively. At $P=0$ the frequency of the bare LO phonon is located in the region of the falling edge arising from the maximum-frequency TA(K)+LA(K) combination. As pressure increases, the LO phonon frequency increases faster than that of the falling edge, thus moving away from the TA(K)+LA(K) region into a region of lower DOS. The decrease of A(LO) by about a factor of 2 (Fig. 7) indicates that the average squared matrix element $|V_3(\mathrm{LO})|^2$ depends on the character of the relevant two-phonon states. The TO linewidth is mainly determined by the anharmonic decay into TA(L)+LA(L) combinations. With pressure the bare TO mode shifts into a region of larger density of TA(L)+LA(L) states. This is considered to be the main reason for the increase of the TO linewidth with pressure. Similarly, the increase of the linewidth of the LO(γ) mode with pressure above 2 GPa can be attributed to a density of states effect. In this case, the LO phonon, after having passed the two-phonon TA(K)+LA(K) edge, moves into the region of enhanced TA(K)+TO(K) DOS, causing a reduction of its lifetime with increasing pressure.

The TO mode can be better fitted at higher than at lower pressures, where a shoulder not observed experimentally appears in the calculated Raman spectra, arising from the TA(L)+LA(L) combination. A better agreement between the experimental and calculated TO structures is obtained if we use a slightly different δ parameter, indicating that the structure due to the TA(L)+LA(L) is located several wave numbers below the value obtained from the calculation with the SM1 and in better agreement with the value shown by the

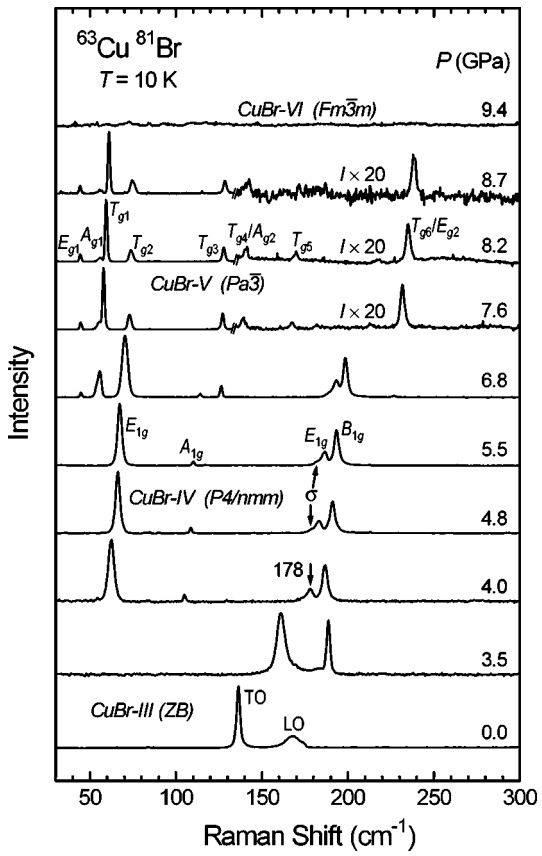

FIG. 9. Low-temperature Raman spectra of ^{63}Cu^{81}Br measured at different pressures up to 10 GPa. Four different phases occur in this pressure range: CuBr-III (zinc blende) up to 4 GPa, CuBr-IV (antilitharge type) between 4 and 7.3 GPa, CuBr-V (SC16) between 6.3 and 8.8 GPa, and CuBr-VI (rocksalt) above 8.8 GPa. The spectra are normalized with respect to the height of the strongest peak at each pressure (except the topmost spectrum).

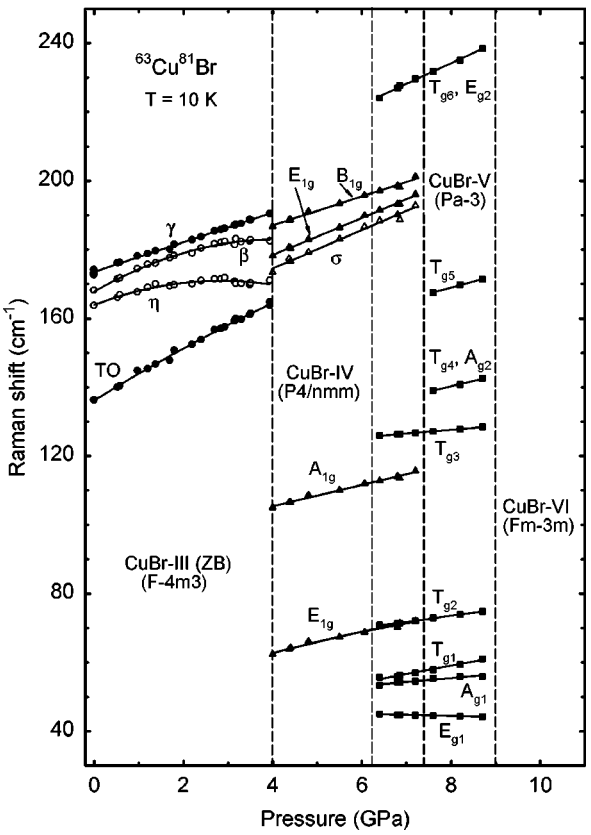

FIG. 10. Frequencies of Raman peak maxima of ^{63}Cu^{81}Br as a function of pressure. Vertical dashed lines mark the pressures where the Raman spectra measured for increasing pressure indicate the appearance or disappearance of phases. The coexistence of phases CuBr-IV and CuBr-V is observed between 6.3 and 7.4 GPa.

calculation with the SM2, which seems to fit better the L-point phonon frequencies.[45] In this context we note that the small decrease of the A(TO) value for intermediate pressures (Fig. 7) is an artifact of the fit procedure caused by the crossing of the TO phonon line through the TA(L)+LA(L) peak of the SM1.

The satisfactory description of the pronounced pressure dependence of the LO- and TO-like features in CuBr by a realistic FRM suggests that the unusual spectral shapes observed at ambient pressure are caused by third-order anharmonic interactions only. This conclusion clearly supports the interpretation of recent isotope substitution experiments on CuBr at ambient pressure.[6] Both the isotope substitution and pressure experiments on CuBr demonstrate that the spectral shapes observed in first-order Raman spectra are highly sensitive to details of the $\mathbf{q}=0$ two-phonon density of states. This also applies to recent experimental and theoretical studies of Raman anomalies of CuCl and GaP.[1–5,10]

IV. HIGH-PRESSURE PHASES

In Fig. 9 we present Raman spectra of ^{63}Cu^{81}Br measured at different pressures up to 10 GPa ($T=10$ K). Three high-pressure phases occur in this pressure range both at room and low temperatures. The frequencies of all observed Raman peak maxima as a function of pressure are displayed in Fig. 10. Above 4 GPa, in phase CuBr-IV, four new Raman modes appear which are clearly resolved in the spectra at 4.0, 4.8, and 5.5 GPa (Fig. 9). The peak at 178.4 cm^{-1} (4 GPa) shows a weak low-energy side band labeled σ. Eight new Raman bands, corresponding to the next phase (CuBr-V) appear above 6.3 GPa. Two of the weaker features were observed only above 7.2 GPa, when the coexisting phase CuBr-IV had disappeared completely. All Raman features disappear near 8.8 GPa, which indicates the completion of the transition to the Raman-inactive rocksalt phase (CuBr-VI). The reversibility of the phase transitions occurring above 4 GPa and possible hysteresis effects have not been studied in full detail. It should be noted here that the specific volume difference between CuBr-IV and CuBr-V is rather small (-1.1%) compared to those between CuBr-III and CuBr-IV (-5.9%) and CuBr-V and CuBr-VI (-4.5%).[32]

From Raman spectroscopy we locate the low-temperature transition pressures (for increasing pressure) at 4.0(1) GPa (III-IV transition, coexistence of the two phases was not observed), 6.3(2) GPa (appearance of phase V), 7.3(2) GPa (upper limit for existence of phase IV), and 8.8(2) GPa (completion of the transition to the rocksalt phase). At room temperature we find the corresponding pressure values to be

TABLE II. Pressure shifts of Raman peak frequencies of CuBr-IV (antilitharge phase) at 10 K as obtained from fitting linear relations to the experimental data. The frequencies ω_0 of the Raman peaks are given at 4.0 GPa. The mode Grüneisen parameters were derived using the bulk modulus value $B_0=49(1)$ GPa (Ref. 32).

Mode	ω_0 (cm^{-1})	$d\omega/dP$ (cm^{-1}/GPa)	γ_G
$E_{1g}(1)$	62.7(4)	2.87(14)	2.24(8)
A_{1g}	105.4(4)	3.09(12)	1.44(6)
σ	174.5(9)	5.6(2)	1.57(6)
$E_{1g}(2)$	178.4(2)	5.4(1)	1.48(4)
B_{1g}	187.0(3)	4.21(14)	1.10(5)

4.7(1), 7.0(2), 8.0(2), and 9.6(2) GPa, respectively. These pressures are in agreement with room-temperature x-ray-diffraction,[49] neutron-diffraction,[32] and optical studies.[30,31] Our low-temperature results for the phase-transition pressures to CuBr-IV [4.0(1) GPa] and CuBr-V [6.3(2) GPa] agree with those reported by Reimann *et al.*,[31] who have measured the pressure dependence of exciton emission spectra in CuBr at 6 K using a DAC with helium as a pressure medium. The coexistence between CuBr-IV and CuBr-V in the pressure range between 6.3 and 7.3 GPa was not observed by these authors, probably because the luminescence decay channel of both phases have very different lifetimes.

A summary of observed Raman peak frequencies and their fitted pressure coefficients for CuBr-IV and CuBr-V is given in Tables II and III, respectively. The assignment of the Raman features given in the tables is explained below.

The four-coordinated structure CuBr-IV has tetragonal symmetry.[26,32,49] The space group is $P4/nmm$.[32] Similar structures are adopted by the natural litharge mineral (PbO),[50] SnO,[51] and the high-pressure phase CuI-V.[32,52] Contrary to PbO and SnO, the copper halides crystallize in the antilitharge structure. The close relationship between the $P4/nmm$ and ZB structures of CuBr and CuI is demonstrated in Fig. 5 of Ref. 27. In the tetragonal structure, the bromine ions undergo a small displacement in the [001] direction with respect to their positions in the ZB phase. The volume of the tetragonal cell is doubled compared to that of the ZB phase. This leads to a BZ of the tetragonal phase which is halved along the [001] direction. Therefore phonons at the X point of the ZB phase are folded into the Γ point of the tetragonal phase.

TABLE III. Pressure shifts of Raman peak frequencies for CuBr-V (SC16 phase). The frequencies ω_0 of the Raman peaks are given at 6.3 GPa. The mode Grüneisen parameters are based on a bulk modulus value $B_0=64(1)$ GPa (Ref. 32). Grüneisen parameters for the isostructural phase CuCl-IV from Ref. 34 are also listed.

Mode	ω_0 (cm^{-1})	$d\omega/dP$ (cm^{-1}/GPa)	γ_G	γ_G (CuCl-IV)
E_{g1}	45.02(4)	−0.313(15)	−0.44(6)	3.28(15)
A_{g1}	53.4(5)	1.13(14)	1.35(14)	1.90(20)
T_{g1}	55.7(3)	2.42(15)	2.78(8)	
T_{g2}	70.9(9)	1.78(6)	1.61(6)	
T_{g3}	126.0(1)	1.10(4)	0.56(5)	0.84(20)
T_{g4},A_{g2}	135.3(2)	3.1(2)	1.47(8)	1.36(25)
T_{g5}	163.3(2)	3.56(16)	1.39(6)	1.6(4)
T_{g6},E_{g2}	224.1(5)	5.99(18)	1.71(5)	1.75(15)

A comparison of Raman spectra of CuBr-IV with those of CuI-V (Refs. 27 and 29) allows us to tentatively assign the four intense Raman peaks observed for CuBr-IV. In the order of increasing frequency, they are attributed to the E_{1g}, A_{1g}, E_{1g}, and B_{1g} modes, as indicated in Fig. 10. These modes correspond, respectively, to the original TA(X), LA(X), TO(X), and LO(X) modes of the ZB phase. The original ZB TO(Γ) and LO(Γ) modes become ungerade modes (E_u and A_{2u}) in the tetragonal phase and are only infrared active. The additional feature σ was observed at 174.5 cm^{-1} at 4 GPa. It exhibits a pressure shift similar to that of the 178.4-cm^{-1} mode. The origin of the σ feature remains unexplained.

The values of mode Grüneisen parameters for CuBr-IV (calculated using the bulk modulus value at 295 K as obtained from neutron-diffraction experiments[32]) are listed in Table II. The Grüneisen parameters of the E_{1g} modes in CuBr-IV (2.24 and 1.48) do not differ much from the corresponding values of CuI-V (2.48 and 1.23, respectively) as calculated from the pressure dependence of Raman mode frequencies at 100 K (Ref. 29) using a bulk modulus $B_0=50(2)$ GPa (Ref. 32).

The structure of CuBr-V belongs to space group $Pa\bar{3}$ which has also been assigned to the high-pressure phase CuCl-IV (Ref. 32) and to a high-pressure modification of GaAs.[53] This structure type, denoted SC16, contains 16 atoms in the cubic unit cell and is the binary analog of the BC8 structure (space group $Ia\bar{3}$) of the metastable phases Si-III (Ref. 54) and Ge-IV.[55] From group theory, ten Raman-active modes (two one-dimensional A_g modes, two two-dimensional E_g modes, and six three-dimensional T_g modes) are expected for the SC16 structure. We have observed up to eight modes for CuBr-V. In the case of the structurally related CuCl-IV, only six Raman modes could be observed.[34] The assignment of the modes of CuBr-V given in Table III is based on a comparison of our experimental results with those for CuCl-IV and with the calculated mode frequencies of CuCl-IV obtained from a rigid ion model.[34] For all modes at frequencies above 120 cm^{-1} (T_{g3}, T_{g4}, A_{g2}, T_{g5}, E_{g2}, and T_{g6}) the assignment is supported by similar values of Grüneisen parameters for CuBr-V and CuCl-IV (see Table III). The different sign and magnitude of the Grüneisen parameters for the lowest-energy feature in CuBr-V and CuCl-IV indicates a possible error in the assignment of the two lowest-energy modes in CuCl-IV. The modes assigned as E_{g1} and A_{g1} in CuCl-IV may actually be the T_{g1} and T_{g2} modes as suggested by their Grüneisen parameters. The negative pressure shift of the lowest energy mode in CuBr-V would be consistent with that of TA modes in zinc-blende semiconductors.

V. SUMMARY

Low-temperature Raman spectra of isotopically pure CuBr ($^{63}Cu^{81}Br$) were measured under hydrostatic pressures up to 10 GPa. The anomalous line shape of the LO scattering in the zinc-blende phase (0–4 GPa) undergoes major changes under pressure and develops into a narrow spectral feature whereas the TO mode is found to broaden considerably. These effects are attributed to changes in the third-order anharmonic coupling of the optical modes with $\mathbf{q}=0$ two-phonon combinations of phonons at lower energies. More specifically, with increasing pressure the bare LO mode shifts into a region of reduced two-phonon DOS, causing a reduction of the anharmonic coupling, and the TO mode shifts into a region of increased two-phonon DOS, leading to an enhancement of the anharmonic decay and a reduction of the phonon lifetime. We showed that all observed spectral changes can be fully accounted for by a Fermi resonance model in combination with a realistic description of the experimental phonon dispersion curves. We conclude that the low-temperature Raman anomalies are mainly due to anharmonic coupling.

Consequently, the anomalous Raman response of CuBr seen *at low temperature* should not be used when looking for support of theoretical models like those of Refs. 7–9 which focus on static or dynamic disorder effects. Other properties of zinc-blende CuBr like the large mean-square displacements of Cu atoms,[56–59] the ionic conductivity,[60,61] and temperature- or pressure-driven structural instabilities appear to be more suitable for testing such kind of theoretical studies.

Our results for the transition pressures to the phases CuBr-IV ($P4/nmm$), CuBr-V ($Pa\bar{3}$) and CuBr-VI (rocksalt) basically agree with those reported earlier.[31,32] The Raman spectra of CuBr-IV and CuBr-V exhibit similarities to those of the structurally related phases CuI-V (Ref. 29) and CuCl-IV. On the basis of these similarities and earlier theoretical calculations of Raman mode frequencies of CuCl-V we propose an assignment of the Raman modes observed in the two four-coordinated high-pressure phases of CuBr.

ACKNOWLEDGMENTS

F.J.M. acknowledges financial support from the European Union under Contract No. HPMF-CT-1999-00074. J.S. acknowledges support from the Max-Planck-Gesellschaft and the Ministerio de Educación y Ciencia (Spain) through the Plan Nacional de Formación del Personal Investigador. The authors thank U. Oelke, W. Dietrich, and U. Engelhardt for technical assistance.

*Corresponding author; email address: k@syassen.de

[1] A. Göbel, T. Ruf, M. Cardona, C. T. Lin, and J. C. Merle, Phys. Rev. Lett. **77**, 2591 (1996).
[2] A. Göbel, T. Ruf, C. T. Lin, M. Cardona, J. C. Merle, and M. Joucla, Phys. Rev. B **56**, 210 (1997).
[3] C. Ulrich, A. Göbel, K. Syassen, and M. Cardona, Phys. Rev. Lett. **82**, 351 (1999).
[4] F. Widulle, T. Ruf, A. Göbel, E. Schönherr, and M. Cardona, Phys. Rev. Lett. **82**, 5281 (1999).
[5] S. Ves, I. Loa, K. Syassen, F. Widulle, and M. Cardona, Phys. Status Solidi B **223**, 241 (2001).
[6] J. Serrano, F. Widulle, T. Ruf, C. T. Lin, and M. Cardona, *Proceedings of the XXV International Conference on the Physics of Semiconductors*, Osaka, 2000 (in print); Phys. Rev. B (to be published).
[7] S. H. Wei, S. B. Zhang, and A. Zunger, Phys. Rev. Lett. **70**, 1639 (1993).
[8] C. H. Park and D. J. Chadi, Phys. Rev. Lett. **76**, 2314 (1996).
[9] S. R. Bickham, J. D. Kress, L. A. Collins, and R. Strumpf, Phys. Rev. Lett. **83**, 568 (1999).
[10] A. Debernardi, Solid State Commun. **113**, 1 (2000), and references therein.
[11] B. A. Weinstein, Solid State Commun. **20**, 999 (1976).
[12] I. P. Kaminow and E. H. Turner, Phys. Rev. B **5**, 1564 (1972).
[13] T. Murahashi, T. Koda, Y. Oka, and T. Kushida, Solid State Commun. **13**, 307 (1973).
[14] M. Krauzman, R. M. Pick, H. Poulet, G. Hamel, and B. Prevot, Phys. Rev. Lett. **33**, 528 (1974).
[15] M. L. Shand, H. D. Hochheimer, M. Krauzman, J. E. Potts, R. C. Hanson, and C. T. Walker, Phys. Rev. B **14**, 4637 (1976).
[16] B. Hennion, B. Prevot, M. Krauzman, R. M. Pick, and B. Dorner, J. Phys. C **12**, 1609 (1979).
[17] Z. Vardeny and O. Brafman, Phys. Rev. B **19**, 3276 (1979).
[18] Z. Vardeny and O. Brafman, Phys. Rev. B **19**, 3290 (1979).
[19] G. Livescu and O. Brafman, Phys. Rev. B **34**, 4255 (1986).
[20] J. E. Potts, R. C. Hanson, C. T. Walker, and C. Schwab, Solid State Commun. **13**, 389 (1973).
[21] E. H. Turner, I. P. Kaminow, and C. Schwab, Phys. Rev. B **9**, 2524 (1974).
[22] Z. Vardeny and O. Brafman, Phys. Rev. B **21**, 2585 (1980), and references therein.
[23] G. Kanellis, W. Kress, and H. Bilz, Phys. Rev. Lett. **56**, 938 (1986); Phys. Rev. B **33**, 8724 (1986); **33**, 8733 (1986).
[24] M. L. Shand and R. C. Hanson, *Proceedings of the International Conference on Lattice Dynamics*, Paris, 1977, edited by M. Balkanski (Flammarion, Paris, 1978).
[25] J. C. Phillips, Rev. Mod. Phys. **42**, 317 (1970).
[26] L. Merrill, J. Phys. Chem. Ref. Data **6**, 1205 (1977), and references therein.
[27] O. Brafman, M. Cardona, and Z. Vardeny, Phys. Rev. B **15**, 1081 (1977).
[28] S. Ves, D. Glotzel, M. Cardona, and H. Overhof, Phys. Rev. B **24**, 3073 (1981).
[29] A. Blacha, Ph.D. thesis, Universität Stuttgart, 1985.
[30] A. Blacha, N. E. Christensen, and M. Cardona, Phys. Rev. B **33**, 2413 (1986).
[31] K. Reimann and St. Rübenacke, Phys. Rev. B **49**, 11 021 (1994).
[32] S. Hull and D. A. Keen, Phys. Rev. B **50**, 5868 (1994), and references therein.
[33] M. Hoffmann, S. Hull, and D. A. Keen, Phys. Rev. B **51**, 12 022 (1995).
[34] C. Ulrich, K. Syassen, M. Cardona, A. Cros, and A. Cantarero, Phys. Rev. B **60**, 9410 (1999), and references therein.
[35] C. T. Lin, E. Schönherr, A. Schmeding, T. Ruf, A. Göbel, and M.

Cardona, J. Cryst. Growth **167**, 612 (1996).
[36] G. J. Piermarini, S. Block, J. D. Barnett, and R. A. Forman, J. Appl. Phys. **46**, 2774 (1975).
[37] H. K. Mao, J. Xu, and P. M. Bell, J. Geophys. Res. **91**, 4673 (1986).
[38] S. Buchsbaum, R. L. Mills, and D. Schiferl, J. Phys. Chem. **88**, 2522 (1984).
[39] B. A. Weinstein and R. Zallen, in *Light Scattering in Solids*, edited by M. Cardona and G. Guntherodt (Springer-Verlag, Berlin/Heidelberg, 1984), Vol. 4, p. 463.
[40] E. Anastasakis and M. Cardona, in *High Pressure Semiconductor Physics II*, edited by T. Suski and W. Paul (Academic, New York, 1998), Vol. 55, p. 117.
[41] J. Ruvalds and A. Zawadowski, Phys. Rev. B **2**, 1172 (1970), and references therein.
[42] H. D. Hochheimer, M. L. Shand, J. E. Potts, R. C. Hanson, and C. T. Walker, Phys. Rev. B **14**, 4630 (1976).
[43] A. A. Maradudin and A. E. Fein, Phys. Rev. **128**, 2589 (1962).
[44] J. Menéndez and M. Cardona, Phys. Rev. B **29**, 2051 (1984), and references therein.
[45] S. Hoshino, Y. Fujii, J. Harada, and J. D. Axe, J. Phys. Soc. Jpn. **41**, 965 (1976).
[46] P. Plumelle, D. N. Talwar, M. Vandevyver, K. Kunc, and M. Zigone, Phys. Rev. B **20**, 4199 (1979).
[47] J. P. Plendl, A. Hadni, J. Claudel, Y. Henninger, G. Morlot, P. Strimer, and L. C. Mansur, Appl. Opt. **5**, 397 (1966).
[48] D. Olego, M. Cardona, and P. Vogl, Phys. Rev. B **25**, 3878 (1982).
[49] J. M. Tranquada and R. Ingalls, Phys. Rev. B **34**, 4267 (1986).
[50] J. Leciejewicz, Acta Crystallogr. **14**, 1304 (1961).
[51] W. Moore and L. Pauling, J. Am. Chem. Soc. **63**, 1392 (1941).
[52] V. Meisalo and M. Kalliomaki, High Temp.-High Press. **5**, 663 (1973).
[53] M. I. McMahan, R. J. Nelmes, D. R. Allan, S. A. Belmonte, and T. Bovornratanaraks, Phys. Rev. Lett. **80**, 5564 (1998).
[54] J. S. Kasper and S. M. Richards, Acta Crystallogr. **17**, 752 (1964).
[55] R. J. Nelmes, M. I. McMahan, N. G. Wright, D. R. Allan, and J. S. Loveday, Phys. Rev. B **48**, 9883 (1993).
[56] S. Miyake and S. Hoshino, Rev. Mod. Phys. **30**, 172 (1958).
[57] B. Prevot, C. Carabatos, C. Schwab, B. Hennion, and F. Moussa, Solid State Commun. **13**, 1725 (1973).
[58] F. Altorfer, B. Graneli, P. Fischer, and W. Buhrer, J. Phys.: Condens. Matter **6**, 9949 (1994).
[59] D. Yang and S. Joo, J. Phys. Soc. Jpn. **66**, 3102 (1997).
[60] J. B. Boyce, T. M. Hayes, and J. C. Mikelsen, Jr., Phys. Rev. B **23**, 2876 (1981).
[61] S. Hull and D. A. Keen, J. Phys.: Condens. Matter **8**, 6191 (1996).